Pramana – J. Phys. (2019) 92:14
https://doi.org/10.1007/s12043-018-1689-8

A numerical investigation of time-dependent MHD axisymmetric transport of Sisko fluid towards elongating porous disk

TARIQ MAHMOOD[1,*], Z IQBAL[1] and AZEEM SHAHZAD[2]

[1]Department of Mathematics, Faculty of Sciences, HITEC University, Taxila 44700, Pakistan
[2]Faculty of Basic Sciences, University of Engineering and Technology, Taxila 44700, Pakistan
*Corresponding author. E-mail: 12-phd-mt-005@hitecuni.edu.pk

MS received 19 October 2017; revised 23 May 2018; accepted 14 June 2018; published online 2 January 2019

Abstract. In this paper, we examined the unsteady boundary layer flow and heat transfer of a Sisko fluid model over an axisymmetric stretching porous disk in the presence of uniform magnetic field. Mathematical modelling is performed in cylindrical polar coordinates. By means of suitable transformations, the governing time-dependent partial differential equations are reduced to nonlinear coupled ordinary differential equations. Shooting method with Runge–Kutta of order 5 is employed to compute non-dimensional velocity and temperature. The effects of pertinent parameters are portrayed through graphs. The skin friction coefficient and Nusselt number are tabulated to study the behaviours at the stretching surface.

Keywords. Axisymmetric flow; time-dependent flow; magnetohydrodynamics; porous radial disk; numerical solutions.

PACS Nos 44.25.+f; 47.10.ad; 47.50.−d

1. Introduction

The analysis of non-Newtonian fluids is very important for scientists, practicing engineers and theoretical mathematicians. Metallurgical and chemical engineers have to cope with different non-Newtonian fluids involving very complex structures. It is difficult to capture various characteristics of non-Newtonian fluids and so far, different models have been proposed in the literature, and Sisko fluid model [1] is one of them. It can describe the shear thinning/shear thickening effects. It has been examined experimentally to fit accurately the viscosity data of different commercial greases [2]. Other models such as power-law and Powell–Eyring models cover only narrow ranges of shear rate. The Sisko model can easily predict a wide range of shear rate. In spite of its diverse applications in industry, only a few works are available [3–7].

Ludwing Prandtl [8] was the first to introduce the idea of boundary layer. It plays a significant role in designing the equipment. It reduces the complicated fluid flow problems into simple ones; moreover, their results agree with the experimental data accurately. Boundary layer flows due to stretching surfaces have earned great interest of the investigators during the last few decades. It occurs in several engineering processes such as in aerodynamics, cooling and drying of paper, extrusion of plastic sheets and glass fibre production. Sakiadis [9] analysed a momentum transfer occurring in the boundary layer adjacent to a continuous sheet moving steadily in an otherwise quiescent fluid environment. After the initial work of Sakiadis [9], it has attracted the attention of many researchers. The boundary layer flow over stretching surfaces was first examined by Crane [10]. He extended the work of Sakiadis by assuming that the velocity of the sheet varies linearly with distance from the slit and determined the closed-form analytic solution for self-similar equations. Schowalter [11] discussed similar solutions to boundary layer flow to power-law pseudoplastic fluids. Andersson and Dandapat [12] examined the flow of a power-law fluid over a linear stretching surface. Some excellent work on boundary layer flows of non-Newtonian fluids over stretching surfaces is available in the literature [13–16].

Many studies of the boundary layer flow over a stretching surface were restricted to steady-state conditions, whereas the unsteady state appears more practically interesting in certain problems. Sharidan *et al* [17] and Mukhopadhyay [18] discussed similar solutions for unsteady flow and heat transfer over a stretching sheet.

All the aforementioned work are concerned with boundary layer flows with heat transfer of Newtonian or non-Newtonian fluids with planar stretching. However, to the best of our knowledge, no attempts have thus far been made to study unsteady boundary layer flow of a Sisko fluid with heat transfer over a radial disk. The governing boundary layer equations are transformed into self-similar nonlinear ordinary differential equations, before being solved numerically by the shooting method. The shooting method is a powerful technique, which yields an approximate numerical solution and has been successfully applied to different kinds of nonlinear problems [19–21].

2. Physical description of the problem

We take two-dimensional (r, z) magnetohydrodynamic boundary layer flow and heat transfer of an incompressible Sisko fluid over an unsteady porous radial stretching disk placed at $z = 0$. The uniform time-dependent magnetic field is applied perpendicular to the disk. The applied transverse magnetic field is assumed to be of variable kind and is given as $B(t) = B_0/(1-\alpha t)^{1/2}$. The flow is induced by stretching of surface with velocity of the form $u = cr/(1-\alpha t)$, in which c is a non-negative real number. Here, it is assumed that the magnetic field is sufficiently weak and we ignore the magnetic induction effects. The flow occurs due to the unsteady stretching of disk along the radial direction (figure 1).

The governing boundary layer equations for the flow and heat transfer of the Sisko fluid in the two-dimensional form are as follows:

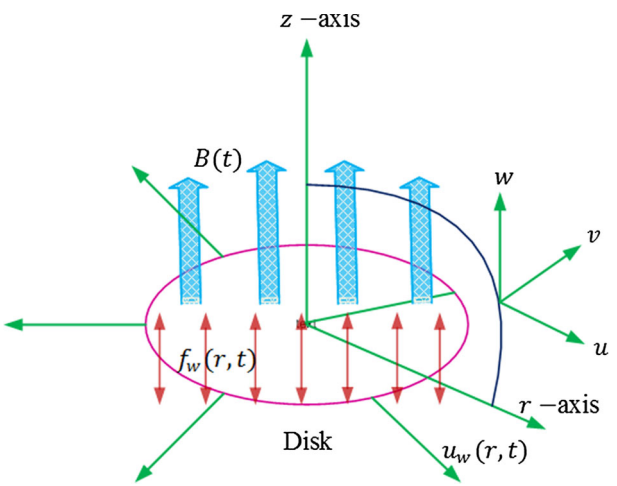

Figure 1. Physical lay-out of the problem with coordinate system.

$$\frac{\partial u}{\partial r} + \frac{u}{r} + \frac{\partial w}{\partial z} = 0, \tag{1}$$

$$\frac{\partial u}{\partial t} + u\frac{\partial u}{\partial r} + w\frac{\partial u}{\partial z} = \frac{a}{\rho}\left(\frac{\partial^2 u}{\partial z^2}\right) - \frac{b}{\rho}\frac{\partial}{\partial z}\left(-\frac{\partial u}{\partial z}\right)^n - \frac{\sigma B_0^2}{\rho}u, \tag{2}$$

$$\frac{\partial T}{\partial t} + u\frac{\partial T}{\partial r} + w\frac{\partial T}{\partial z} = \frac{k}{\rho c_p}\frac{\partial^2 T}{\partial z^2}. \tag{3}$$

The corresponding boundary conditions are

$$\begin{aligned} u &= U_w(r,t) = \frac{cr}{1-\alpha t}, \\ w &= -f_w(r,t), \quad T = T_w \quad \text{at } z = 0, \\ u &\to 0, \quad T \to T_\infty \quad \text{as } z \to \infty, \end{aligned} \tag{4}$$

where ρ is the density of the fluid, σ is the electrical conductivity, T is the temperature of the fluid, k is the thermal conductivity and c_p is the specific heat. The stretching velocity $U_w(r,t)$, porosity of the surface S and surface temperature $T_w(r,t)$ are taken as

$$\begin{aligned} u_w(r,t) &= \frac{cr}{1-\alpha t}, \quad T_w(r,t) = T_\infty + \frac{dr}{1-\alpha t}, \\ f_w(r,t) &= U_w(r,t)\,\frac{2n}{n+1}\mathrm{Re}_b^{-1/(n+1)}, \\ S &= \left(\frac{3n+1}{n+1}\right)\frac{\mathrm{Re}_b^{1/(n+1)}}{U_w} f_w, \end{aligned} \tag{5}$$

where α, d and c denote the constants with $c > 0$, $d \geq 0$ and $\alpha \geq 0$ and (with $\alpha t < 1$). Note that α has a dimension of time^{-1}. Here $(n > 0)$, a and b are the material constants, u and w are the velocity components along the r and z directions, respectively, U_w is the stretching surface velocity, $S > 0$ for mass suction and $S < 0$ for mass injection, T_∞ is the ambient temperature, and $T_w > T_\infty$. To facilitate the analysis, we introduce the subsequent conventional transformation and dimensionless variable η and $f(\eta)$ in the following form:

$$\begin{aligned} \psi(r,z) &= -\frac{cr^3}{1-\alpha t}\mathrm{Re}_b^{-1/(n+1)} f(\eta), \\ u &= \frac{-1}{r}\frac{\partial \psi}{\partial z}, \quad w = \frac{1}{r}\frac{\partial \psi}{\partial r}, \\ \theta(\eta) &= \frac{T - T_\infty}{T_w - T_\infty}, \quad \eta = \frac{z}{r}\mathrm{Re}_b^{1/(n+1)}, \\ \mathrm{Re}_b &= \frac{r^n U_w^{2-n}}{b/\rho}. \end{aligned} \tag{6}$$

Thus, the velocity components can be written as

$$u = U_w f'(\eta)$$

and

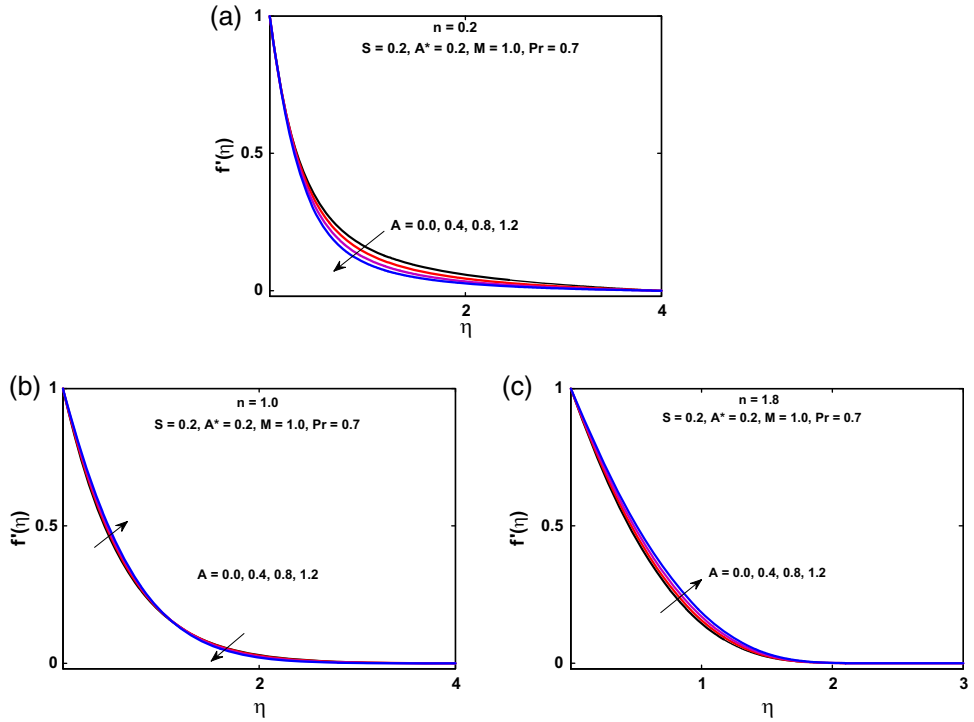

Figure 2. (**a**)–(**c**) Effects of unsteadiness parameter A on $f'(\eta)$.

$$w = -U_w \mathrm{Re}_b^{-1/(n+1)} \frac{1}{n+1}[(3n+1)\, f(\eta) + (1-n)\, \eta f'(\eta)]. \tag{7}$$

By using the above transformations, the governing equation (1) is identically satisfied and eqs (2) and (3) along with boundary conditions given in eq. (4) are transformed to a non-dimensional form as follows:

$$A^* f''' + A\left(f' + \frac{2-n}{n+1}\eta f''\right) + n\left(-f''\right)^{n-1} f''' - \frac{3n+1}{n+1} f f'' + f'^2 + M f' = 0, \tag{8}$$

$$\frac{\theta''}{\mathrm{Pr}} + \frac{3n+1}{n+1} f\theta' - f'\theta - A\left[\theta + \left(\frac{2-n}{n+1}\right)\eta\theta'\right] = 0, \tag{9}$$

$$f(0) = S, \quad f'(0) = 1, \quad f'(\infty) \to 0,$$
$$\theta(0) = 1, \theta(\infty) \to 0, \tag{10}$$

where ψ is the stream function, $A = \alpha/c$ is the unsteadiness parameter and for $A = 0$, problems reduce to a steady-state situation. M is the Hartman number, Pr is the generalised Prandtl number, A^* is the ratio of two Reynolds numbers and the definition of these dimensionless parameters is

$$M = \frac{\sigma B_0^2}{\rho c}, \quad A^* = \frac{\mathrm{Re}_b^{2/(n+1)}}{\mathrm{Re}_a},$$

$$\mathrm{Pr} = \frac{\rho c_p r U_w}{k} \mathrm{Re}_b^{-2/(n+1)}. \tag{11}$$

The physical quantities of interest such as skin friction coefficient C_f and local Nusselt number Nu_r are defined as

$$C_f = \frac{\tau_w}{\frac{1}{2}\rho u_w^2}, \quad \mathrm{Nu}_r = \frac{r q_w}{k(T_w - T_\infty)}, \tag{12}$$

where τ_w and q_w from the disk are

$$\tau_w = \left(a + b\left|\frac{\partial u}{\partial z}\right|^{n-1}\right)\frac{\partial u}{\partial z}\bigg|_{z=0},$$
$$q_w = -k\left(\frac{\partial T}{\partial z}\right)\bigg|_{z=0}. \tag{13}$$

In view of eq. (6), the dimensionless form of eqs (10) and (11) becomes

$$\frac{1}{2}\mathrm{Re}_b^{1/(n+1)} C_f = A^* f''(0) - \left[-f''(0)\right]^n,$$
$$\mathrm{Re}_b^{-1/(n+1)} \mathrm{Nu}_r = -\theta'(0). \tag{14}$$

3. Computational procedure

The shooting method along with the Runge–Kutta fifth-order technique was incorporated to tackle the system of nonlinear differential equations. Thus, the solution of coupled nonlinear governing boundary

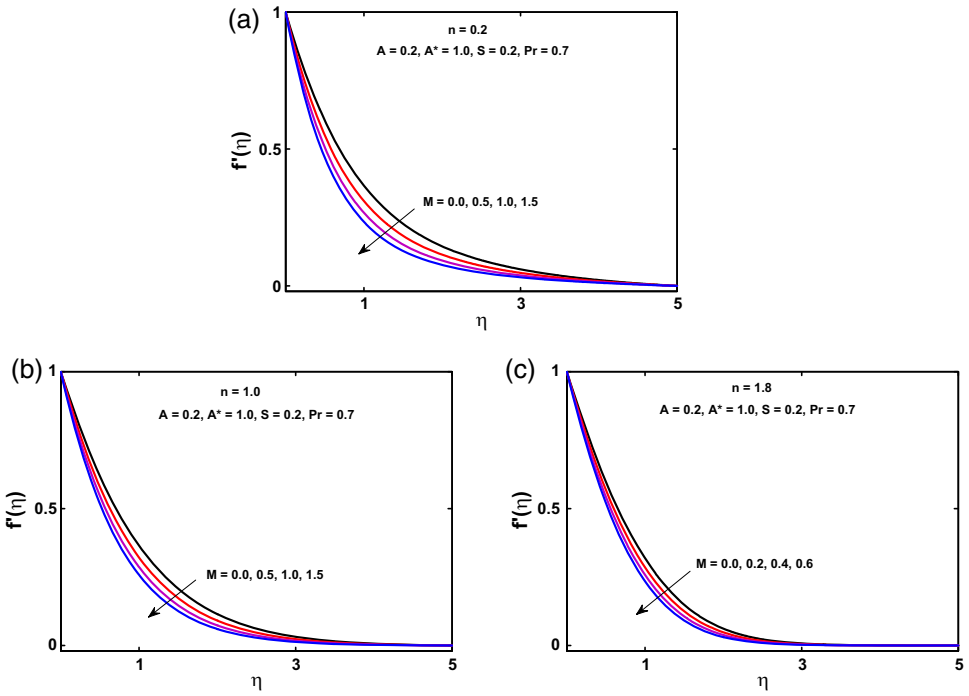

Figure 3. (**a**)–(**c**) Effects of magnetic parameter M on $f'(\eta)$.

layer equations (8) and (9) together with boundary conditions (10) is computed by means of the shooting method along the Runge–Kutta fifth-order technique. Initially, higher order nonlinear differential equations (8) and (9) are converted into a system of first-order differential equations and further transformed into an initial value problem by labelling the variables as

$$\begin{aligned}&\left(f, f', f'', f''', \theta, \theta'\right)^{\mathrm{T}}\\&\quad = (y_1, y_1' = y_2, y_2' = y_3, y_3' = y_4,\\&\qquad y_4' = y_5, y_5' = y_6)^{\mathrm{T}}.\end{aligned}$$

According to our numerical procedure, the above system of equations is of the form

$$\begin{pmatrix} f \\ f' \\ f'' \\ f''' \\ \theta \\ \theta' \\ \theta'' \end{pmatrix} = \begin{pmatrix} y_1 \\ y_2 \\ y_3 \\ \dfrac{\left[\frac{3n+1}{n+1} y_1 y_3 - A\left(y_2 + \frac{2-n}{n+1}\eta y_3\right) - y_2^2 - M y_2\right]}{\left(A^* + n(-y_3)^{n-1}\right)} \\ y_4 \\ y_5 \\ \mathrm{Pr}\, y_2 y_4 - \frac{3n+1}{n+1}\mathrm{Pr}\, y_1 y_5 \\ \quad + A\,\mathrm{Pr}\left[y_4 + \left(\frac{2-n}{n+1}\right)\eta y_5\right] \end{pmatrix}, \tag{15}$$

with boundary conditions

$$\begin{pmatrix} y_1(0) \\ y_2(0) \\ y_2(\infty) \\ y_4(0) \\ y_4(\infty) \end{pmatrix} = \begin{pmatrix} S \\ 1 \\ U_1 \\ 1 \\ U_2 \end{pmatrix}. \tag{16}$$

The above nonlinear coupled ordinary differential equations (ODEs) along with initial conditions are solved using the Runge–Kutta method of order 5 integration technique. Appropriate values of unknown initial conditions U_1 and U_2 are approximated through Newton's method until boundary conditions $f'(\eta) \to 1$, $f''(\eta) \to 0$, $\theta(\eta) \to 0$ as $\eta \to \infty$ are satisfied. Computations are carried out using the mathematics software MATLAB. The end of a boundary layer region, i.e. when $\eta = \infty$ to each group of parameters, is determined when the values of unknown boundary conditions at $y = 1$ do not change to a successful loop with an error less than 10^{-6}.

4. Theoretical results analysis

Nonlinear ordinary differential equations (8) and (9) subject to boundary equations (10) have been solved numerically by the shooting method. The variations of pertinent parameters on velocity and temperature distribution are discussed in detail and shown in figures 2–12 graphically. The physical lay-out of the boundary layer thickness near the disk can be seen

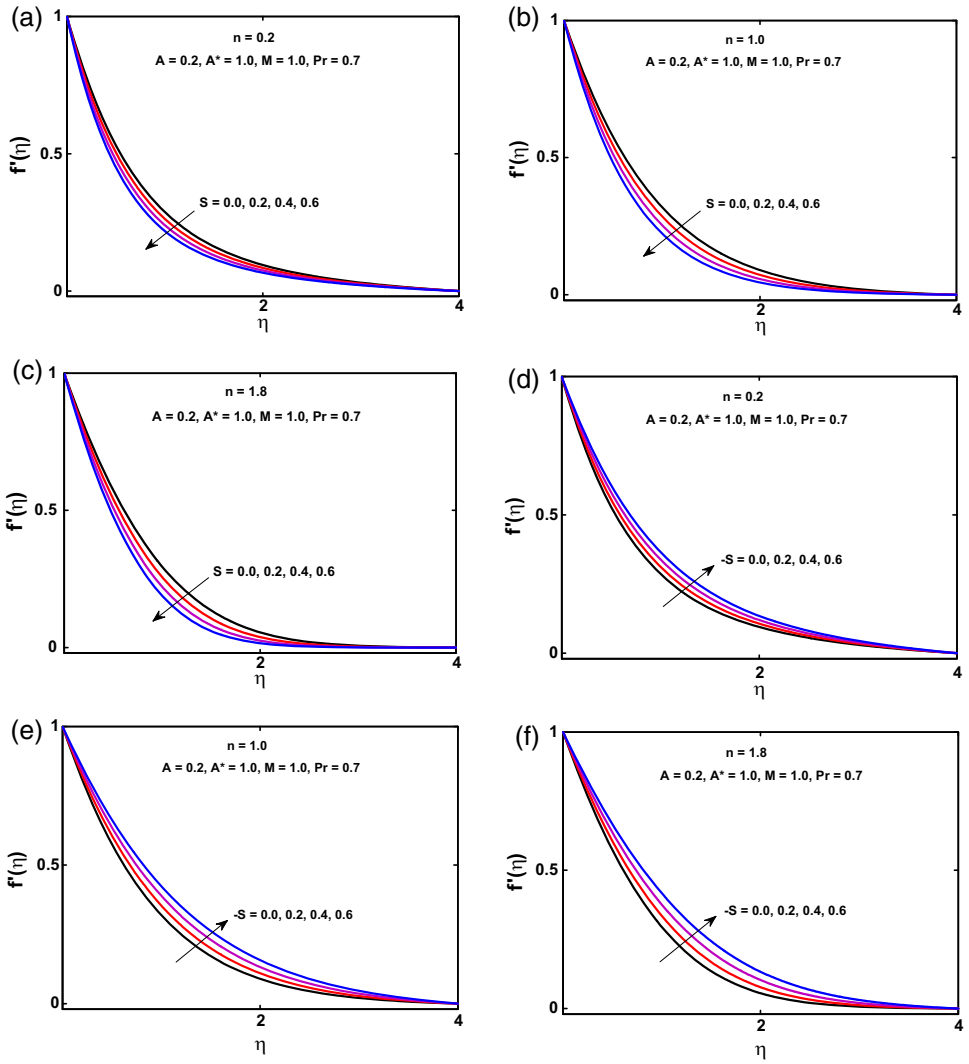

Figure 4. (**a**)–(**c**) Effects of suction parameter S on $f'(\eta)$. (**d**–**f**) Effects of injection parameter $-S$ on $f'(\eta)$.

by observing the velocity profile. The effects of unsteadiness parameter A on the velocity profile are examined in figures 2a–2c. It showed quite different behaviour for shear thinning, Newtonian and shear thickening fluids, an increase in unsteadiness parameter A decreases the boundary layer for pseudoplastic or shear thinning fluid ($n < 1$) whereas for Newtonian ($n = 1$) it showed mixed behaviour, i.e. half of a region increases and half of a region decreases, for dilatant or shear thickening ($n > 1$) fluid, it increases the velocity hence the boundary layer thickness. Furthermore, it is observed that this effect is more prominent in the case of shear thinning/thickening fluid compared to the Newtonian fluid. The variations of magnetic parameter M on velocity profile are shown in figures 3a–3c for all pseudoplastic (shear thinning fluid) ($n < 1$), Newtonian ($n = 1$) and dilatant (shear thickening) ($n > 1$) fluids. It is evident from these figures that an increase in the magnetic parameter M causes a decrease in the velocity profile and boundary layer thickness, which indicates that the rate of transport is considerably reduced with an increase in magnetic parameter M. It concludes that the transverse magnetic field opposes transport phenomena. This is due to the fact that the variation of magnetic parameter leads to variation of Lorentz force, which creates resistance to transport phenomena. Figures 4a–4c and 4d–4f are plotted to see the effects of suction/injection S on the velocity profile for pseudoplastic (shear thinning fluid) ($n < 1$), Newtonian ($n = 1$) and dilatant (shear thickening) ($n > 1$) fluids. These figures elucidate that the suction ($S > 0$) acts to increase the adherence of fluid to the surface which in turn retards the flow and causes a decrease in the velocity and boundary layer thickness for all pseudoplastic, Newtonian and dilatant fluids and a quite opposite trend is seen in the case of

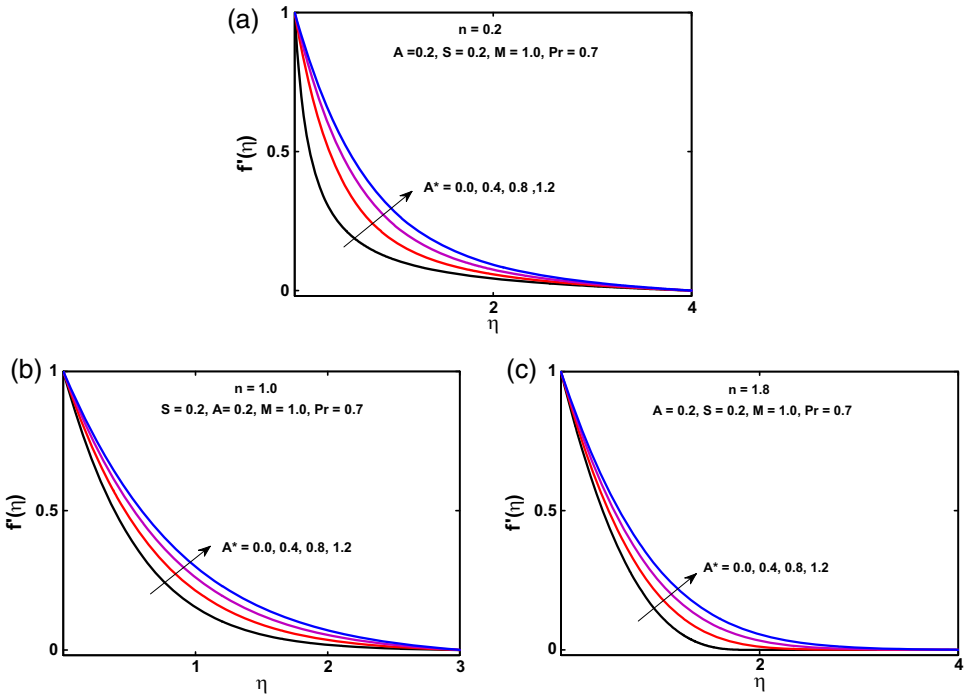

Figure 5. (**a**)–(**c**) Effects of material parameter A^* on $f'(\eta)$.

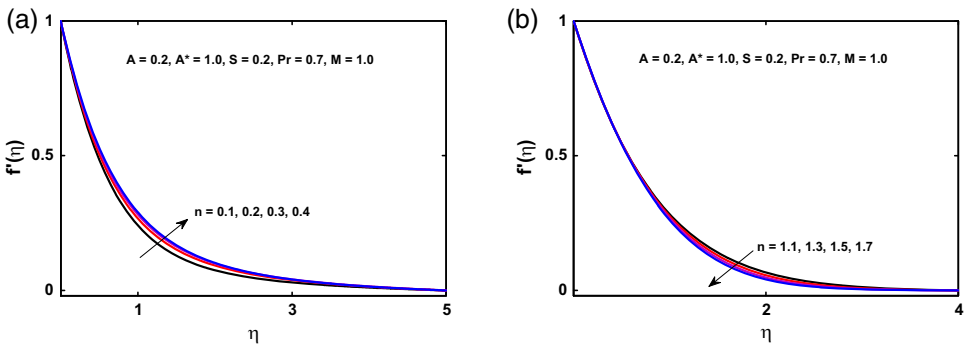

Figure 6. (**a**), (**b**) Effects of power-law index n on $f'(\eta)$.

injection ($S < 0$). Figures 5a–5c describe the influence of material parameter A^* on velocity profile. From these figures it is observed that an increase in material parameter A^* causes an increase in velocity and boundary layer thickness. Figures 6a and 6b show the effects of power-law index n on velocity profile. It is observed that the velocity profile decreases for increasing values of power-law index n for both the pseudoplastic fluids ($n < 1$) and quite opposite effects were seen for dilatant fluid ($n > 1$). Moreover, a notable influence might be seen for $n < 1$ compared to the case $n > 1$.

The thermal boundary layer structure can be seen by having a look at the temperature distribution. In order to see the variations of unsteadiness parameter A on temperature distribution, figures 7a–7c are plotted. An increase in the unsteadiness parameter A decreases the thermal boundary layer for pseudoplastic or shear thinning fluid ($n < 1$), Newtonian ($n = 1$), dilatant or shear thickening fluids ($n > 1$). Furthermore, it is observed that this effect is more prominent in the case of Newtonian fluid compared to pseudoplastic or dilatant fluid. The effects of the magnetic parameter M on temperature distribution are shown in figures 8a–8c for all pseudoplastic (shear thinning fluid) ($n < 1$), Newtonian ($n = 1$) and dilatant (shear thickening) ($n > 1$) fluids. It is evident from these figures that an increase in the magnetic parameter M causes an increase in the temperature profile and hence the thermal boundary layer thickness increases for shear thinning fluid ($n < 1$), which indicates that the magnetic parameter M is having a direct relationship with temperature profile for the case $n < 1$, whereas for other cases, i.e. Newtonian fluid ($n = 1$) and shear

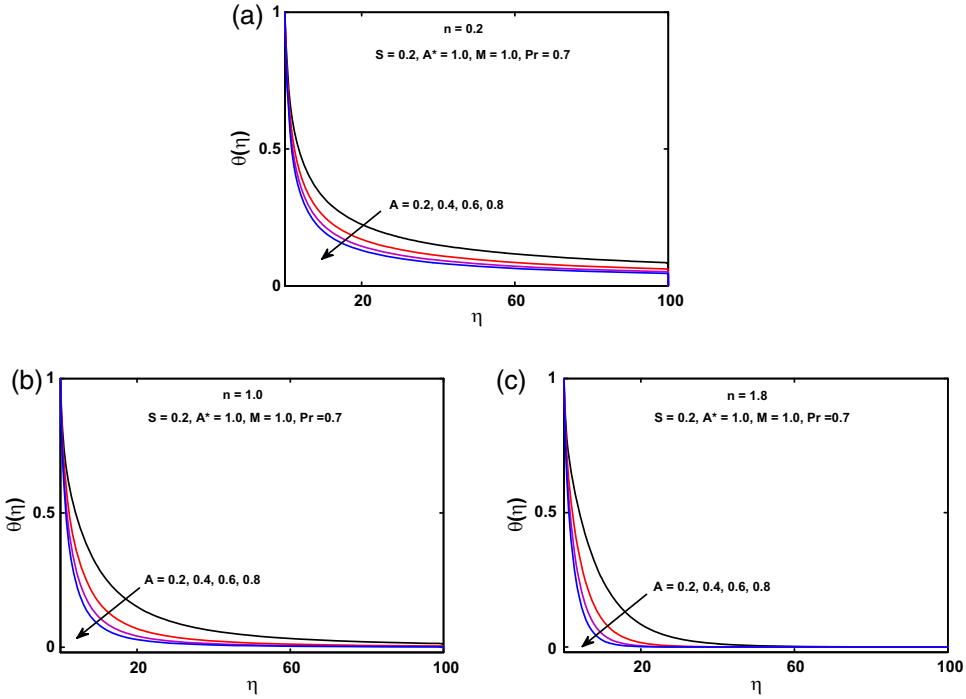

Figure 7. (**a**)–(**c**) Effects of unsteadiness parameter A on $\theta(\eta)$.

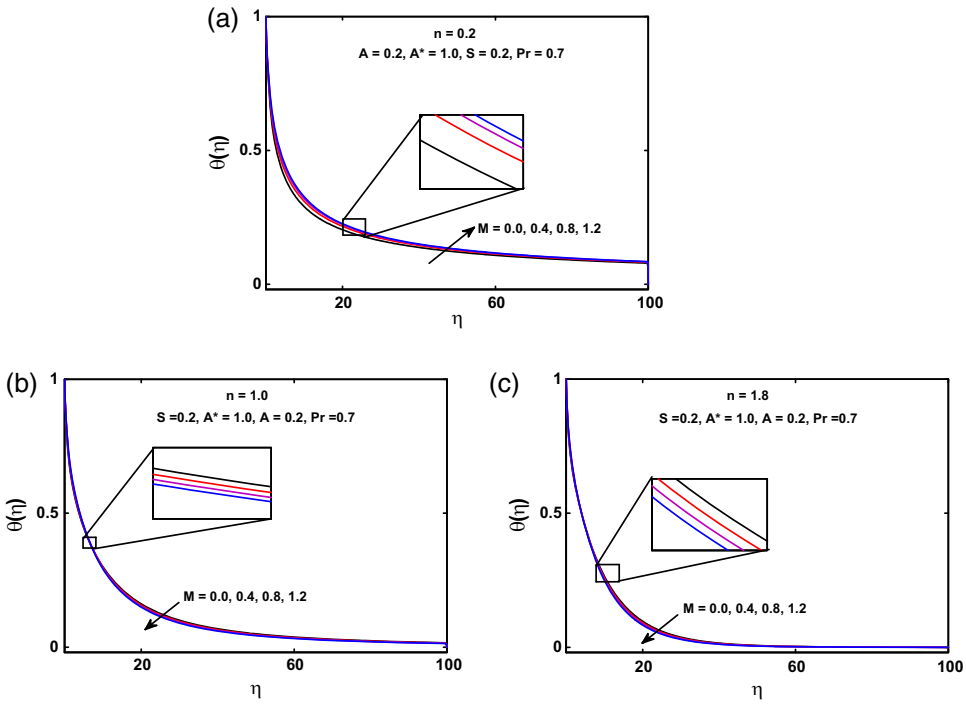

Figure 8. (**a**)–(**c**) Effects of magnetic parameter M on $\theta(\eta)$.

thickening fluid ($n > 1$), it shows the quite opposite behaviour. Figures 9a–9c and 9d–9f are plotted to see the effects of suction/injection S on temperature distribution for pseudoplastic (shear thinning fluid) ($n < 1$), Newtonian ($n = 1$) and dilatant (shear thickening) ($n > 1$) fluids. These figures elucidate that the injection ($S < 0$) acts to increase the adherence of fluid to the surface which in turn causes a decrease in the temperature and thermal boundary layer thickness for all pseudoplastic, Newtonian and dilatant fluids and the opposite trend is witnessed in the case of suction ($S > 0$). Figures 10a–10c describe the influence

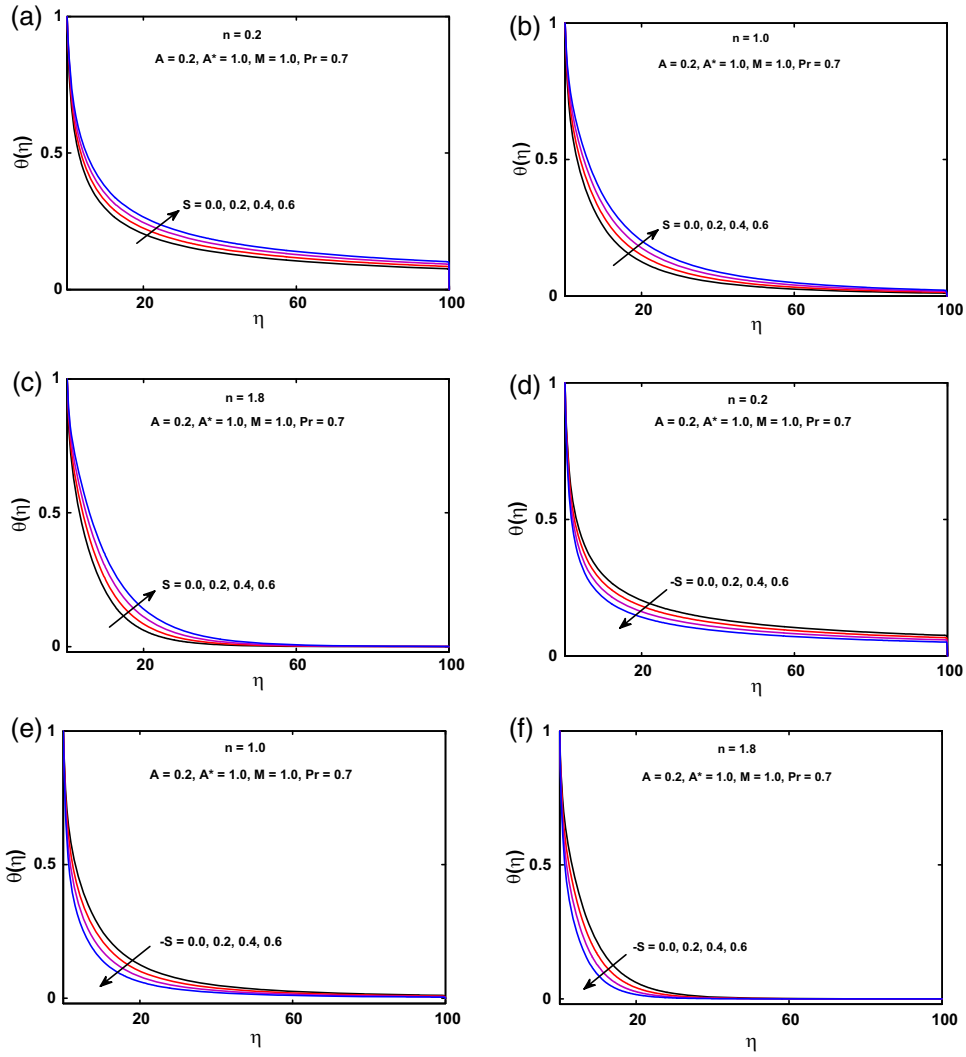

Figure 9. (**a**)–(**c**) Effects of suction parameter S on $\theta(\eta)$. (**d**)–(**f**) Effects of injection parameter S on $\theta(\eta)$.

of material parameter A^* on temperature distribution. From these figures it is observed that an increase in the material parameter A^* causes a decrease in the temperature distribution for shear thinning fluid ($n < 1$), whereas it describes the opposite behaviour for Newtonian ($n = 1$) and shear thickening fluids ($n > 1$). Hence, the thermal boundary layer thickness decreases. Further, we can conclude from these figures that the temperature distribution of Newtonian and dilatant fluids is higher than that of the pseudoplastic fluids. Figures 11a–11c describe the development of generalised Prandtl number Pr on temperature distribution. It is observed from these graphs that an increase in Prandtl number Pr causes an increase in temperature and thermal boundary layer thickness. Figures 12a and 12b show the effects of power-law index n on temperature distribution. It is observed that temperature distribution decreases for increasing values of power-law index n for both pseudoplastic ($n < 1$) and dilatant fluids ($n > 1$). It can be seen from these figures that for $n < 1$ the pseudoplastic or shear thinning fluid power-law index n significantly affects the temperature distribution but marginally for $n > 1$, i.e. dilatant or shear thickening fluids, which determines the evolution of the thermal boundary layer thickness, is thicker for $n < 1$ than for $n > 1$.

The influence of significant physical parameters of interest on the skin friction coefficient C_f is tabulated in table 1. From this table, it is seen that with an increase in unsteadiness parameter A, suction parameter S and magnetic parameter M, the magnitude of skin friction coefficient increases for all pseudoplastic, Newtonian and dilatant fluids, while an increase in material parameter A^* and injection parameter $-S$ causes a decrease in the magnitude of skin friction coefficient.

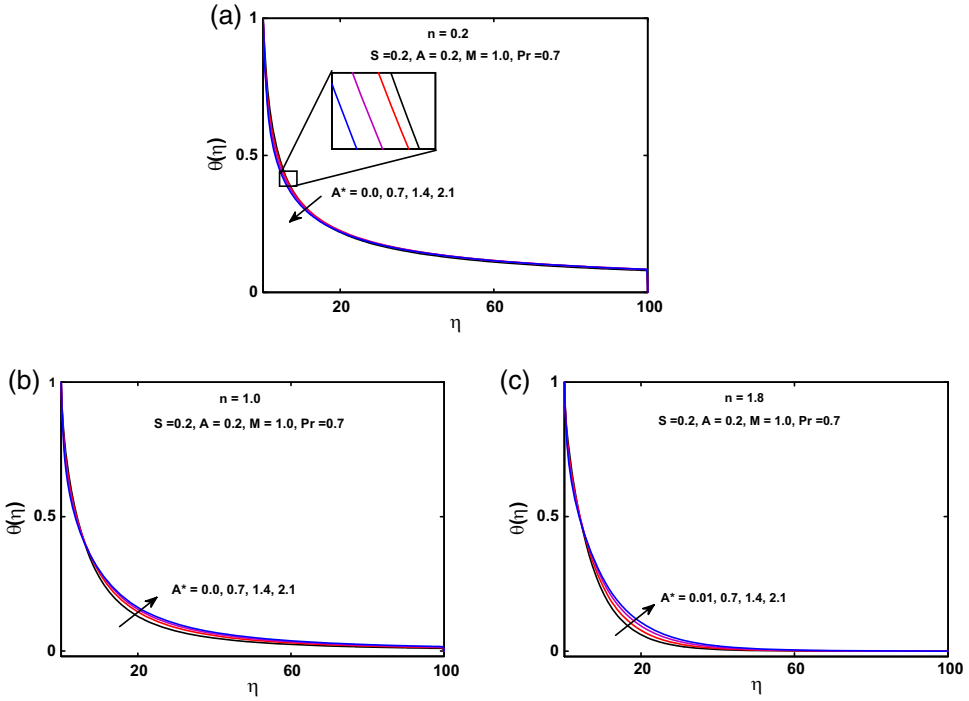

Figure 10. (**a**)–(**c**) Effects of material parameter A^* on $\theta(\eta)$.

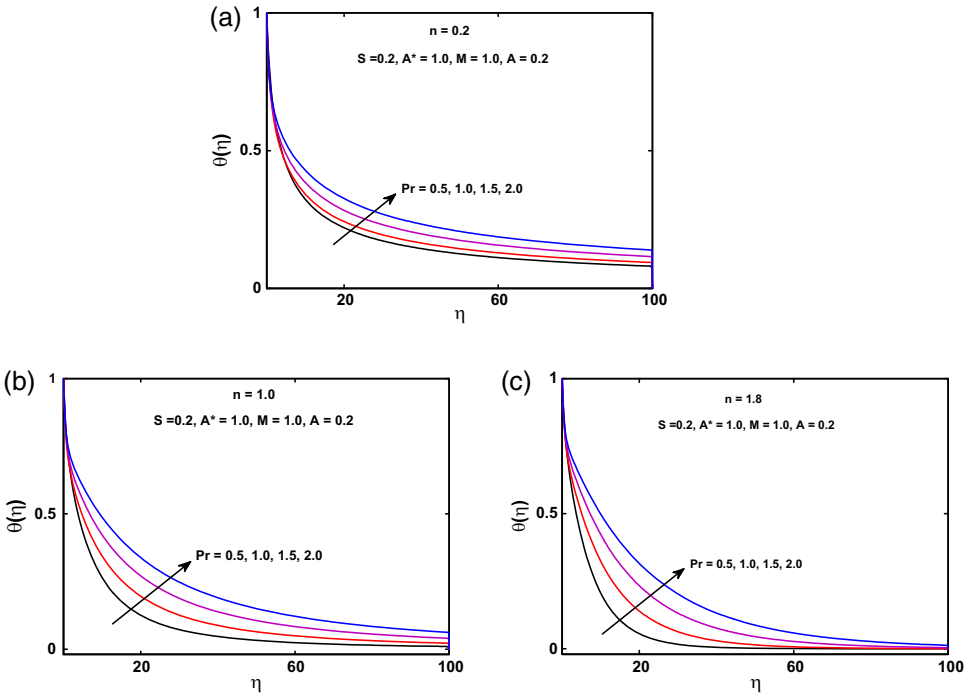

Figure 11. (**a**)–(**c**) Effects of Prandtl number Pr on $\theta(\eta)$.

The variations of different physical parameters of interest on Nusselt number Nu_x are calculated in table 2. From this table, it is to be noted that with an increase in values of unsteadies parameter A, the generalised Prandtl number Pr and suction parameter S, the magnitude of Nusselt number also increases for all pseudoplastic, Newtonian and dilatant fluids, while an increase in magnetic parameter M and injection parameter $-S$ causes a decrease in Nusselt number. Moreover, it is also observed that with an increase in the value

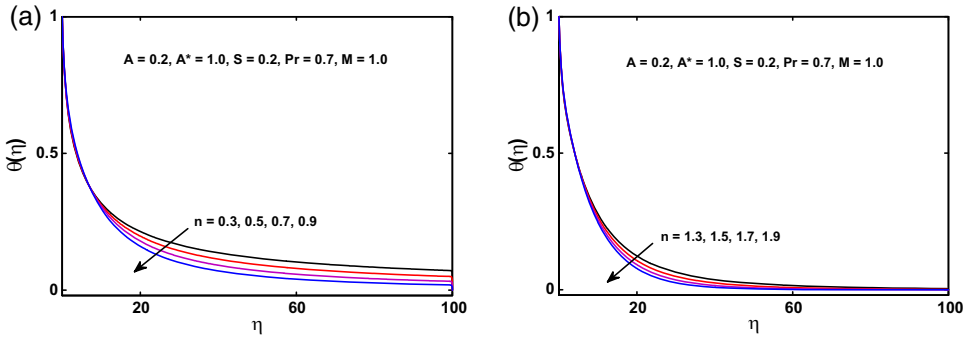

Figure 12. (**a**), (**b**) Effects of power-law index n on $\theta(\eta)$.

Table 1. Numerical values of the skin friction coefficient $\frac{1}{2}\mathrm{Re}_b^{1/(n+1)}C_f$ for significant parameters.

				$-\frac{1}{2}\mathrm{Re}_b^{1/(n+1)}C_f$		
A	M	A^*	S	$n = 0.2$	$n = 1.0$	$n = 1.8$
0.2	1	1	0.4	1.382000	1.538999	1.650000
0.4				1.674999	1.753999	1.820999
0.6				1.967000	1.957000	1.977000
0.2	0			1.227000	1.236000	1.282999
	0.5			1.315000	1.395999	1.472999
	1			1.382000	1.538999	1.650000
	1	0.5		1.577999	1.830000	1.986000
		1.0		1.382000	1.538999	1.650000
		1.5		1.284000	1.348999	1.404999
		1	−0.4	1.222999	1.032999	0.882199
			−0.2	1.259000	1.143000	1.041999
			0.2	1.338999	1.396999	1.426999
			0.4	1.382000	1.538999	1.650000

Table 2. Numerical values of Nusselt number $\mathrm{Re}_b^{-1/(n+1)}\mathrm{Nu}_r$ for significant parameters.

					$\mathrm{Re}_b^{-1/(n+1)}\mathrm{Nu}_r$		
A	M	A^*	S	Pr	$n = 0.2$	$n = 1.0$	$n = 1.8$
0.2	1.0	1.0	0.4	0.7	0.779300	1.576000	1.840000
0.4					0.935299	1.647999	1.895999
0.6					1.057000	1.712999	1.951000
0.2	0.0				0.899000	1.631000	1.869999
	0.5				0.826899	1.602000	1.854000
	1.0				0.779300	1.576000	1.840000
	1.0	0.5			0.693299	1.517000	1.805000
		1.0			0.779300	1.576000	1.840000
		1.5			0.743099	1.551999	1.826999
		1.0	−0.4		0.482599	0.646199	0.757199
			−0.2		0.536400	0.815799	0.970399
			0.2		0.680800	1.290000	1.517000
			0.4		0.779300	1.576000	1.840000
			0.4	0.5	0.737099	1.545000	1.778999
				0.7	0.779300	1.576000	1.840000
				1.0	0.867099	1.621000	1.928000

of material parameter A^*, shear thinning and shear thickening fluids show mixed behaviour.

5. Conclusions and novelty of the paper

The boundary layer flow and heat transfer of a Sisko fluid over an unsteady porous radially stretching sheet are investigated in the presence of magnetic field. Using appropriate transformations, the governing coupled partial differential equations were reduced to an ordinary differential equation. The numerical solution of reduced differential equations was calculated using the shooting method. Some of the important findings of the investigation are listed as follows:

- The inside boundary layer value of power-law index n significantly affects the velocity profile but marginally affect the temperature profile.
- An increase in unsteadiness parameter A for $0 \leq n < 1$, magnetic parameter M and mass suction parameter $S > 0$ reduces the velocity profile.
- An increase in mass injection parameter $S < 0$, material parameter A^* and unsteadiness parameter A for $1 \leq n < 2$ enhances the velocity profile for different values of power-law index n.
- The velocity profile and temperature profile showed a similar behaviour for unsteadiness parameter A for $0 \leq n < 1$, material parameter A^* and power-law index n for $n \geq 1$ whereas opposite effects are noted for unsteadiness parameter A for $1 \leq n < 2$, suction/injection parameter S and magnetic parameter M.
- The magnitude of skin friction increases with an increase in unsteadiness parameter A, magnetic parameter M and suction parameter S and decreases with an increase in material parameter A^* and injection parameter $-S$ for different values of power-law index n.
- An increase in injection parameter $-S$ and magnetic number M results in a decrease in the magnitude of Nusselt number, whereas the magnitude of Nusselt number increases for an increase in suction parameter S, unsteadiness parameter A and the generalised Prandtl number Pr for different values of power-law index n.

References

[1] A W Sisko, *Ind. Eng. Chem. Res.* **50**, 1789 (1958)
[2] A W Sisko, *J. Colloid Sci.* **15**, 89 (1960)
[3] R M Turian, T W Ma, F L G Hsu and M D J Sung, *Int. J. Multi. Flow* **24**, 225 (1998)
[4] A M Siddiqui, M Ahmed and Q K Ghori, *Chaos Solitons Fractals* **33**, 1006 (2007)
[5] Y Wang, T Hayat, N Ali and M Oberlack, *Physica A* **387**, 347 (2008)
[6] H M Mamboundou, M Khan, T Hayat and F M Mahomed, *J. Porous Med.* **12**, 695 (2009)
[7] M Khan, Q Abbas and K Duru, *Int. J. Numer. Methods Fluids* **62**, 1169 (2010)
[8] L Prandtl, *Verhandlungen des dritten internationalen mathematiker-kongresses* (Leipzig, Druck und Verlag Von B.G., Teubner, Heidelberg, 1904)
[9] B C Sakiadis, *AIChE J.* **7**, 26 (1961)
[10] L J Crane, *Z. Angew. Math. Phys.* **21**, 645 (1970)
[11] W R Schowalter, *AIChE J.* **6**, 24 (1960)
[12] H I Andersson and B S Dandapat, *Stability Appl. Anal. Continuous Media* **11**, 339 (1991)
[13] M Pakdemirli, *IMA J. Appl. Math.* **50**, 133 (1993)
[14] R Cortell, *Appl. Math. Comput.* **168**, 557 (2005)
[15] M Yurusoy, *Int. J. Eng. Sci.* **44**, 325 (2006)
[16] C Wang and I Pop, *J. Non-Newtonian Fluid Mech.* **138**, 161 (2006)
[17] S Sharidan, T Mahmood and I Pop, *Int. J. Appl. Mech. Eng.* **11**, 647 (2006)
[18] S Mukhopadlyay, *Int. J. Heat Mass Transfer* **52**, 3261 (2009)
[19] S Xun, J Zhao, L Zheng, X Chen and X Zhang, *Int. J. Heat Mass Transfer* **103**, 1214 (2016)
[20] G C Dash, R S Tripathy, M M Rashidi and S R Mishra, *J. Mol. Liq.* **221**, 860 (2016)
[21] N Acharya, K Das and P K Kundu, *J. Mol. Liq.* **225**, 418 (2017)